

Aggregation-Induced Emission Mechanism of Dimethoxy-Tetraphenylethylene in Water Solution: Molecular Dynamics and QM/MM Investigations

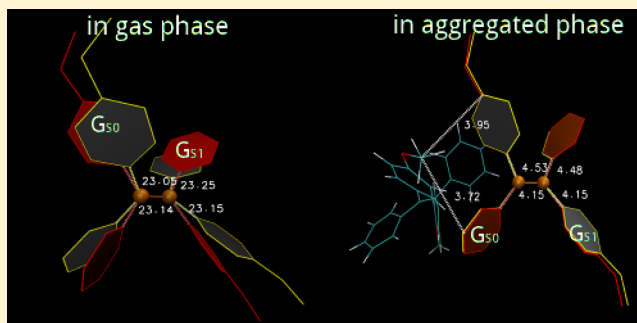
Guangxu Sun,[†] Yi Zhao,^{*,‡} and WanZhen Liang^{*,‡}

[†]Department of Chemical Physics, University of Science and Technology of China, Hefei, 230026 Anhui, China

[‡]State Key Laboratory of Physical Chemistry of Solid Surfaces, Collaborative Innovation Center of Chemistry for Energy Materials, and Department of Chemistry, College of Chemistry and Chemical Engineering, Xiamen University, Xiamen, 361005 Fujian, China

S Supporting Information

ABSTRACT: Molecular dynamics simulations and combined quantum mechanics and molecular mechanics calculations are employed to investigate dimethoxy-tetraphenylethylene (DMO-TPE) molecules in water solution for their detailed aggregation process and the mechanism of aggregation-induced emission. The molecular dynamics simulations show that the aggregates start to appear in the nanosecond time scale, and small molecular aggregates appear at low concentration; whereas the large aggregates with a chain-type structure appear at high concentration, and the intramolecular rotation is largely restricted by a molecular aggregated environment. The average radical distribution demonstrates that the waters join the aggregation process and that two types of hydrogen bonds between DMO-TPE and water molecules are built with the peaks at about 0.5 and 0.7 nm, respectively. The spectral features further reveal that the aggregates dominantly present J-type aggregation although they fluctuate between J-type and H-type at a given temperature. The statistical absorption, emission spectra, and the aggregation-induced emission enhancement with respect to the solution concentration agree well with the experimental measurements, indicating the significant effect of molecular environments on the molecular properties.



1. INTRODUCTION

Most organic conjugated molecules commonly present a bright emission in a dilute solution and become nonemissive in an aggregate state.^{1–4} This phenomenon is known as aggregation-caused quenching. In 2001, however, Tang's group⁵ found a new organic chromophore whose emission effect exhibits an exactly opposite behavior, and this phenomenon has been named as the aggregation-induced emission (AIE). Since then, many investigations have rapidly expanded this field to reveal the corresponding mechanism (see, for instance, refs 6 and 7) and explore a number of practical applications, such as in organic light-emitting diodes (OLEDs), chemosensors, and biosensors.^{8–16}

The tetraphenylethylene (TPE) molecule and its derivatives are among the selected class of chromophores which exhibit the remarkable AIE effect.¹⁷ Due to the easy synthesis and simple structures, they are often chosen as the candidates for applications, as well as the investigation of the AIE mechanism to guide further efforts in the development of new AIE materials with high luminescence efficiencies.^{6,7,18–28} Within a wealth of accessible mechanisms for AIE phenomena,^{7,29–33} the restricted intramolecular rotation (RIR)^{34–43} has been well recognized as a dominant mechanism in the TPE chromophores.^{7,17,44–47} After photoexcitation, an isolated TPE

molecule in gas phase or in dilute solution generally presents the intramolecular rotations of low-frequency phenyl torsion modes and C=C twist modes that open a nonradiative relaxation channel for the excited-state energy decay. The molecular aggregation may restrict these rotations, resulting in the deactivated nonradiative channel and enhanced emission. The detailed excited-state dynamics of the TPE molecule had been further studied by experimental measurements and theoretical investigations,^{23,32,44,45,48} and those nonradiation and radiation rates have been also quantitatively calculated from the perturbation theory together with quantum mechanics/molecular mechanics (QM/MM) at the molecular geometries in gas phase and solid-state environment.^{49,50} The results have shown that the low-frequency motions are indeed associated with the nonradiative energy dissipations.

In this paper, we investigate the detailed aggregation process of dimethoxy-tetraphenylethylene (DMO-TPE) molecules in solution and the concentration-dependent behavior of the AIE effect by using molecular dynamics (MD) simulations and QM/MM calculations. The DMO-TPE^{17,21,51} has been experimentally synthesized and demonstrated that its fluo-

Received: October 21, 2014

rescence emission in acetonitrile (AN) is barely discernible, whereas the suspensions in water/AN mixtures with high water fractions are highly emissive because of the molecular aggregation in water. The AIE effect has also been theoretically explained by the RIR at the DMO-TPE geometry cut from the X-ray diffraction crystal structure (CCDC 622769).¹⁷ However, it is still unclear for us how the aggregates are formed in solution, how the solution concentration affects the performed aggregation structures and the AIE effect, and whether the solvent molecules join the aggregation process and produce the aggregation structures different from those in the solid-state crystal with the pure chromophores. The above information should be significant for the synthesizing of controllable AIE aggregates. In the present work, therefore, we first try to answer the questions mentioned above by the MD simulation which has the benefit that the microscopic dynamic process at an atomic level can be revealed for large systems. In the MD simulations, we choose the different DMO-TPE concentrations in water to investigate the aggregation processes. These calculations may mimic the experimental condition with respect to the water fractions in water/AN mixtures where the higher water fraction corresponds to more DMO-TPE molecules which can join molecular aggregation. Many interesting results are indeed obtained from the simulations, such as the aggregation time, the concentration-dependence of aggregation structures, and the hydrogen bond performance between DMO-TPE and water molecules.

Once the geometrical structures of DMO-TPE aggregates are obtained, their electronic structures, absorption, and emission spectra are readily obtained from quantum chemistry calculations. Here, we use the QM/MM method to explicitly account for the explicit molecular environment. We first consider an isolated DMO-TPE molecule and, then, investigate the changes of its electronic structures and spectra in gas phase and solution. More importantly, we will investigate the spectra of DMO-TPE dimers and reveal the aggregational properties, as well as the fluctuation effect of geometries on the spectra. The results will show that the AIE effect is dependent on the solution concentration, which agrees well with the experimental measurement.¹⁷

The paper is arranged as follows. Section 2 outlines the calculation approaches. Section 3 shows the results and discussions. The concluding remarks are given in Section 4.

2. COMPUTATIONAL METHODS

The standard MD simulations are performed in the Gromacs MD software.⁵² The initial geometry of the DMO-TPE molecule is optimized at the theoretical level of B3LYP/6-31G* by using the Gaussian 09 software package.⁵³ Then the optimized DMO-TPE molecules and water molecules are mixed in a cubic box of 6 nm. The number of DMO-TPE molecules are among 10 to 100, dependent on the molecular concentration in water solution, and the number of total water molecules are among 4000 to 7000. The universal force field⁵⁴ is adopted to describe the atom–atom interactions for DMO-TPE molecules. Some of the force field parameters have been modified for the present system according to the results from the electronic structure calculations; the detailed parameters are listed in Table S1 of the Supporting Information (SI). The TIP3P model⁵⁵ for water molecules is applied. The coulomb interaction effect for the whole system is also incorporated with the Particle Mesh Ewald (PME) method^{56,57} with 1.2 nm cutoff. With the constructed models, we start MD simulation

with 1 fs time step under the isothermal–isobaric ensemble (NPT), the most closely to laboratory conditions with a flask open to ambient temperature and pressure, where the reference pressure (1 Torr) and temperature (300 K) effects are incorporated with the Berendsen method.⁵⁸ After 1 ns NPT simulation, we find that the systems are at equilibration and the cubic box becomes a little different. The change of volume of the simulation box lies in the range of 0.3–1.9%, and, then, the canonical ensemble (NVT) is chosen for the next MD simulation. The aggregate geometries from the simulations with the time duration of 10 ns are collected for the statistical analysis of molecular structures and spectra.

At the snapshots of molecular geometries obtained from the MD simulation, the ONIOM method^{59,60} is adopted to calculate the electronic and geometrical structures. We consider one or two DMO-TPE molecules quantum mechanically, and their ground- and excited-state electronic structures are calculated by DFT and TDDFT with DFT xc functional B3LYP. The effect of the remaining DMO-TPE molecules and water molecules in the box are incorporated at the MM level, and electronic embedding is applied in the QM/MM calculations.

For the isolated DMO-TPE molecule in water solution, the integral equation formalism Polarizable Continuum Model (IEPCM)⁶¹ implemented in the Gaussian 09 software package is adopted to map the water environment. For excited-state calculations in solution, there is a distinction between equilibrium and nonequilibrium calculations. The solvent responds in two different ways to changes in the state of the solute: it polarizes its electron distribution, which is a very rapid process, and the solvent molecules reorient themselves (e.g., by a rotation), a much slower process. The geometry optimizations correspond to an equilibrium calculation, which describes a situation where the solvent had time to fully respond to the solute in the above two ways. The vertical excitation energy calculations correspond to a nonequilibrium calculation where the solvent did not have time to fully respond to the solute. We apply the default procedures in the Gaussian 09 software package for TDDFT excited-state geometry optimizations (the equilibrium solvation) and TDDFT energies (the nonequilibrium solvation). The vertical excitation energies calculated by TD-B3LYP/PCM at optimized ground- and first excited-state geometries are used as the absorption and emission energies, respectively. Except where explicitly stated in Table 2, the linear response^{62,63} PCM approach is applied to calculate the excitation energies. Table 2 includes the results calculated by both the linear response and the state-specific PCM^{64,65} approaches.

3. RESULTS AND DISCUSSION

3.1. Properties of the Isolated DMO-TPE Molecule in Vacuo and Solution.

At first we study the geometrical and electronic structures of the isolated DMO-TPE molecule in the ground state (S_0) and first singlet excited state (S_1) in gas phase and water solution. Figure 1 displays its molecular geometry. Table 1 lists the major structural parameters. The four phenyl groups are individually linked to C3 and C4 through single bonds with nearly equal bond lengths. In both S_0 and S_1 states, the molecule has the symmetric character with $\angle C4-C3-C19-C24 = \angle C3-C4-C25-C26$ and $\angle C4-C3-C5-C6 = \angle C3-C4-C12-C13$. The solvent effect slightly affects the molecular geometry, leading to a maximum difference of 2° in the torsional angles between the vacuum and solution

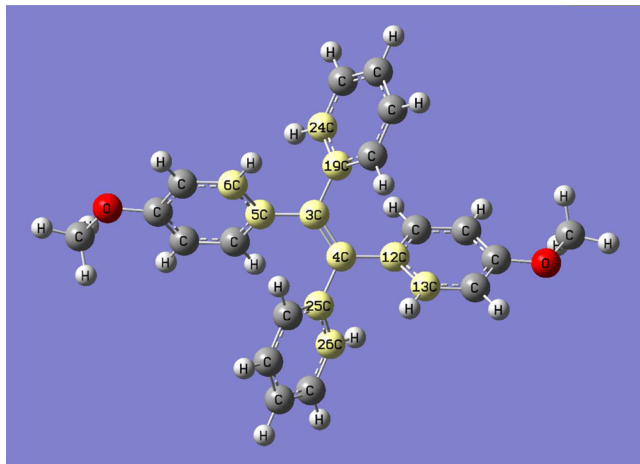


Figure 1. Molecular geometry of DMO-TPE.

molecular environments. This phenomenon reveals that the phenyl rings of isolated DMO-TPE molecule have the freedom to rotate. The rotations may have the effect on the molecular properties. We thus calculate the low-lying excitation energies and the corresponding oscillator strengths of the DMO-TPE molecule in vacuum and water solution, respectively. The results are displayed in Figure 2. Obviously, two absorption line shapes are similar. The solvent effect slightly enhances the light absorption and redshifts the peak positions.

Upon the electronic excitation, the bond length of C3–C4 is largely lengthened, changed from 1.37 to 1.49 Å. The lengths of the bonds which connect C3 or C4 with phenyl groups in S_1 are slightly shortened compared with those in S_0 , but the marked rotations of the phenyl rings occur and the maximum difference of rotational angles reaches to 24° between the S_0 and S_1 geometries. The differences appearing in the dihedral angles $\angle C19-C3-C4-C25$ and $\angle C5-C3-C4-C12$ are even larger, reaching to 55°. Clearly, the electronic excitation magnifies the noncoplanar character of the molecular geometry. The changes on the molecular geometries play an obvious role on the emission energies. A Stokes shift of about 400 nm is observed for the isolated DMO-TPE molecule in both gas phase and water solution (see Table 2). The large Stokes-shift values for the isolated molecule are partially related to the single-excitation nature of the TDDFT method. To prove this, we performed the configuration interaction singles (CIS) and

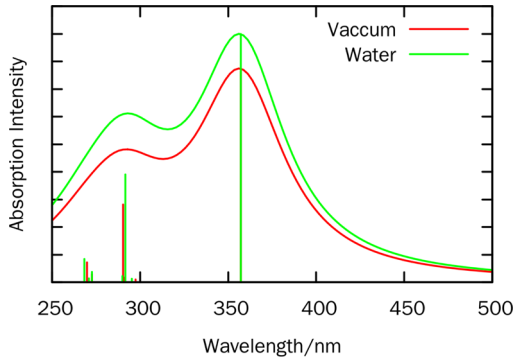


Figure 2. Electronic absorption spectra of the DMO-TPE molecule in vacuo and water solution. The Lorentzian line shape function with the width of 30 nm is adopted.

CIS(D)^{66,67} calculations for the absorption and emission energies of the DMO-TPE molecule in vacuo and find that the vertical excitation energy difference of $\Delta E_{\text{CIS}} - \Delta E_{\text{CIS}(D)}$ at the S_0 geometry is about 0.23 eV, but the difference of calculated emission energies is −0.45 eV. Compared to CIS(D), CIS largely underestimates the emission energy, which indicates that the electronic correlation becomes stronger at the S_1 geometry due to the decrease of dihedral angles $\angle C19-C3-C4-C25$ and $\angle C5-C3-C4-C12$ and that the neglecting of double excitation in CIS and TDDFT results in the underestimated emission energy for the isolated DMO-TPE molecule in both gas phase and water solution. The CIS(D) approach is a perturbative correction to CIS that approximately introduces effects of double excitations for the excited states in a noniterative scheme very similar to the second-order perturbation theory, in which doubly excited states are coupled to the ground state.

To see how the rotation of phenyl groups influences the light emission efficiency, we calculate the change of oscillator strengths along the relaxation pathway. The oscillator strength of the first singlet excited state at each step of the excited-state geometrical relaxation is shown in Figure 3. Obviously, the geometry relaxation starting from the ground-state conformation gradually decreases the oscillator strength of the S_1 state. The oscillator strength in vacuum is smaller than that in water solution, indicating that the solvent effect slightly hinders the rotation of phenyl rings. This phenomenon caused by the

Table 1. Major Geometrical Parameters^a

	vacuum			solution			aggregation		
	G_g	G_e	Δ	G_g	G_e	Δ	G_g	G_e	Δ
$\angle C4-C3-C19-C24$	132.8°	153.5°	20.7°	131.5°	153.2°	21.7°	113.1°	115.2°	2.1°
$\angle C4-C3-C5-C6$	134.8°	158.4°	23.6°	133.2°	157.1°	23.9°	147.8°	152.5°	4.7°
$\angle C3-C4-C25-C26$	132.8°	153.5°	20.7°	131.5°	153.2°	21.7°	138.8°	142.5°	3.7°
$\angle C3-C4-C12-C13$	134.8°	158.4°	23.6°	133.2°	157.1°	23.9°	121.6°	128.2°	6.6°
$\angle C5-C3-C4-C12$	167.1°	110.4°	56.7°	166.9°	111.8°	55.1°	150.9°	140.6°	10.3°
$\angle C19-C3-C4-C25$	166.8°	110.7°	56.1°	166.9°	112.0°	54.9°	158.2°	148.5°	9.7°
C3–C4	1.37	1.49	0.12	1.37	1.49	0.12	1.37	1.44	0.07
C3–C5	1.49	1.45	0.04	1.49	1.44	0.05	1.49	1.45	0.03
C3–C19	1.50	1.45	0.05	1.50	1.45	0.05	1.49	1.48	0.01
C4–C12	1.49	1.45	0.04	1.49	1.44	0.05	1.50	1.47	0.03
C4–C25	1.50	1.45	0.05	1.50	1.45	0.05	1.48	1.45	0.03

^a G_g and G_e denote the optimized geometries of S_0 and S_1 states, respectively. Δ is the difference. The unit of bond length is angstrom. B3LYP/6-31G* is adopted.

Table 2. Absorption, Emission Energies, and Oscillator Strengths of a Single DMO-TPE Molecule in Vacuum, Water Solution, and Aggregates^a

6-31G*	vacuum		solution			aggregation		expt
	$\Delta E/\text{nm}$	f	$\Delta E/\text{nm}$	f	$\Delta E^*/\text{nm}$	$\Delta E/\text{nm}$	f	
Abs.	357.10	0.3824	357.27	0.4498	355.90	346.62	0.4026	330
Emi.	827.44	0.1682	845.88	0.2079	812.54	440.27	0.3906	477
6-311+G(d,p)	vacuum		solution			aggregation		expt
	$\Delta E/\text{nm}$	f	$\Delta E/\text{nm}$	f	$\Delta E^*/\text{nm}$	$\Delta E/\text{nm}$	f	$\Delta E/\text{nm}$
Abs.	366.50	0.3448	366.33	0.4135	365.30	363.68	0.3544	330
Emi.	862.42	0.1593	885.07	0.1979	852.88	464.81	0.3452	477

^a ΔE and f denote the vertical excitation energies and the oscillator strengths; ΔE^* denotes the energy calculated by the state-specific PCM approach.^{64,65}

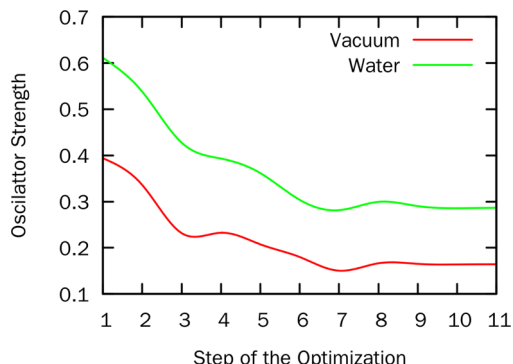


Figure 3. Oscillator strength of first excited state changed vs the excited-state geometrical relaxation. The value is taken from each step of the optimization cycle.

torsional motions can explain the low emission efficiency of the isolated DMO-TPE molecule because of the small oscillator strength at the excited-state geometry, and it also indicates that the emission can be enhanced if the rotations of phenyl rings are hindered, the typical mechanism of AIE.

3.2. Aggregation Pathways of DMO-TPE Molecules.

With the knowledge of the geometries and spectra of an isolated DMO-TPE molecule, we study the properties of aggregates. It is noted that many researchers have used the molecular geometries cut from its crystal structure to investigate the aggregation effect. However, the molecular stack in solution is much more complex, and the aggregate size may heavily depend on the solution concentration. Meanwhile, the understanding of detailed molecular aggregation process is important for the design of the aggregates with tunable properties. In this section, we therefore show the detailed dynamic process for the aggregation and the stacking properties from the MD simulations.

In the model construction for the simulations, we first build the primitive cell including a single DMO-TPE molecule surrounded by water molecules. The number of water molecules in the cell are determined by the concentration. We then fill up the box with the primitive cell periodically and record the aggregation dynamics by combining NPT and NVT simulations. Since the aggregation properties obviously depend on the molecular concentration, here, we select the solution with 1.11 mol % (about 64 DMO-TPE molecules have become involved) as an example to show the aggregation pathways.

To reveal whether water molecules join the aggregation, we display in Figure 4 the radial distribution function (RDF) which describes how the distribution of the mass-center distance between DMO-TPE and water molecules varies at several time

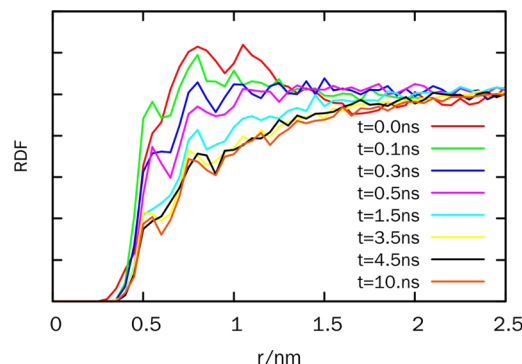


Figure 4. Radial distribution function of the mass-center distance between DMO-TPE and water molecules.

windows. As expected, the water molecules are closely around DMO-TPE molecules in a distance range from 0.5 to 1.3 nm. During the period of 0 to 3.5 ns, the water molecules are away from DMO-TPE molecules, and only one-third of the water molecules remain. After 3.5 ns, the RDF is nearly unchanged, indicating that the aggregates become stable, and the accomplished time for aggregation is about 3.5 ns. Interestingly, the two peaks in the stable RDF appear at about 0.5 and 0.7 nm. The detailed analysis reveals that the peak at 0.5 nm is from the hydrogen bond between the water molecule and phenyl groups of the DMO-TPE molecule, whereas the peak at 0.7 nm is from the hydrogen bond between the water molecule and methoxy groups of the DMO-TPE molecule.

Figure 5 shows the RDF varied as the mass-center distance between two DMO-TPE molecules. The more detailed aggregation processes are shown in Figures S4–S6 in the

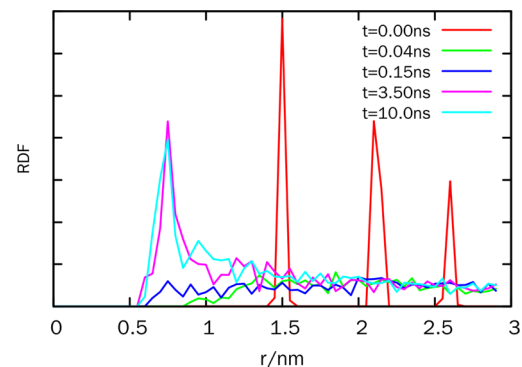


Figure 5. Radial distribution function of the mass-center distance between two DMO-TPE molecules.

Supporting Information. At the initial time, the RDF shows three sharp peaks at 1.5, 2.1, and 2.6 nm, respectively, and each represents our initial molecular arrangement in the box along the *a*, *b*, and *c* axis of the cell. After a very short time (<0.04 ns), those periodical arrangements disappear, and the distribution of DMO-TPE molecules becomes disorder. At 0.15 ns, a peak around 0.7 nm starts to appear, and its intensity reaches a stable value at 3.5 ns. After that, the peak intensity only has a small fluctuation around the stable value. This procedure clearly shows the detailed aggregation dynamics. From the initial distribution, the DMO-TPE molecules soon meet each other in 0.15 ns and begin to aggregate; the stable aggregates appear in 3.5 ns. This RDF clearly demonstrates that at the equilibrium status, the mass-center distance between two neighbor DMO-TPE molecules is around 0.7 nm. At low concentration, the aggregates dominantly have a dimer property because the only one peak exists in the stable configuration.

It is found that the aggregation times are concentration-dependent, but the aggregation pathways are not sensitive to the concentration. We split the whole aggregation time into three pieces. The first piece is from the initially ordered arrangement to the random distribution, the second piece is for starting the aggregation, and the third piece is for finishing the aggregation. Figure 6 shows the concentration dependence of

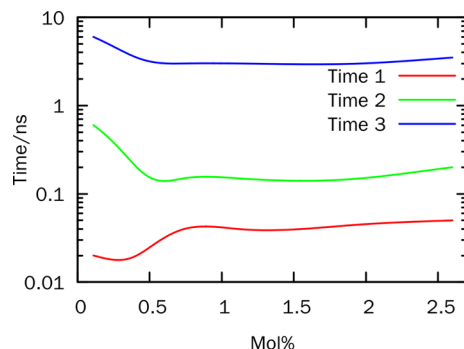


Figure 6. Concentration dependence relationship of three feature times.

three feature times. As expected, at low concentration, the time 1 is about two times shorter than that at high concentration; however, the times 2 and 3 are about three times longer than those at high concentration. Interestingly, those feature times become concentration-independent as the concentration is higher than 1.0 mol %.

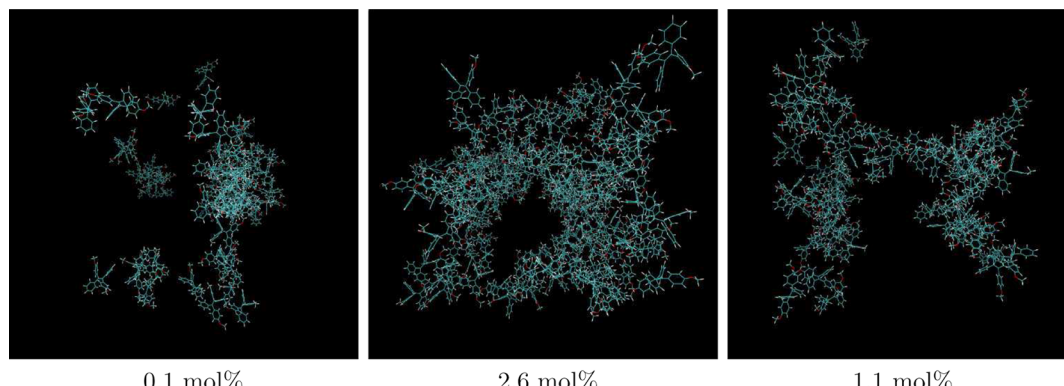


Figure 7. DMO-TPE aggregates at different concentrations.

At high enough concentrations, the time scales of aggregation processes are similar, but the aggregates have obviously different properties. Figure 7 displays the aggregates at the concentration of 0.1, 2.6, and 1.1 mol %, respectively. Obviously, at low concentration, small isolated aggregation blocks are formed, whereas at high concentration, the large aggregates with a chain-type structure are formed. To quantitatively analyze the aggregation properties, we calculate the averaged RDF over the MD trajectory from 3.4 to 10 ns. Figure 8(a) shows these averaged RDFs at several different

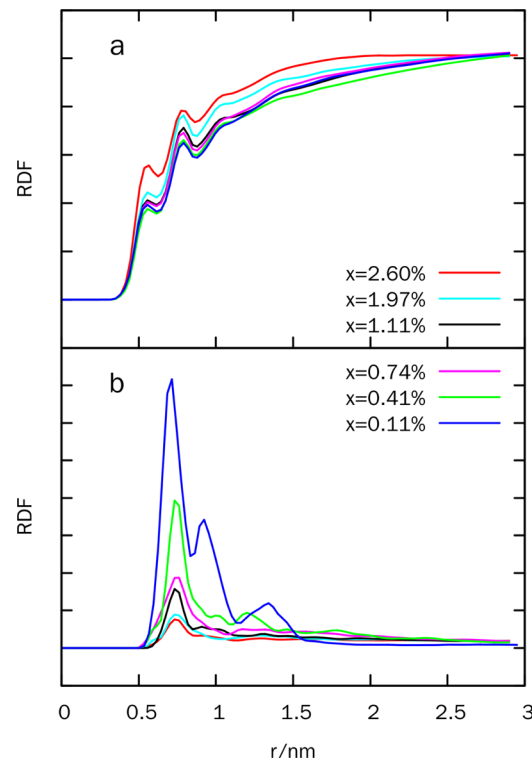


Figure 8. Average radial distribution functions varied as the distances between water and DMO-TPE (a) and between two DMO-TPE molecules (b).

concentrations vs the intermolecular distance between DMO-TPE and waters and (b) vs the intermolecular distance between DMO-TPE and DMO-TPE. It is found that the two types of hydrogen bonds between waters and DMO-TPE molecules always exist in the tested concentration ranges; however, the

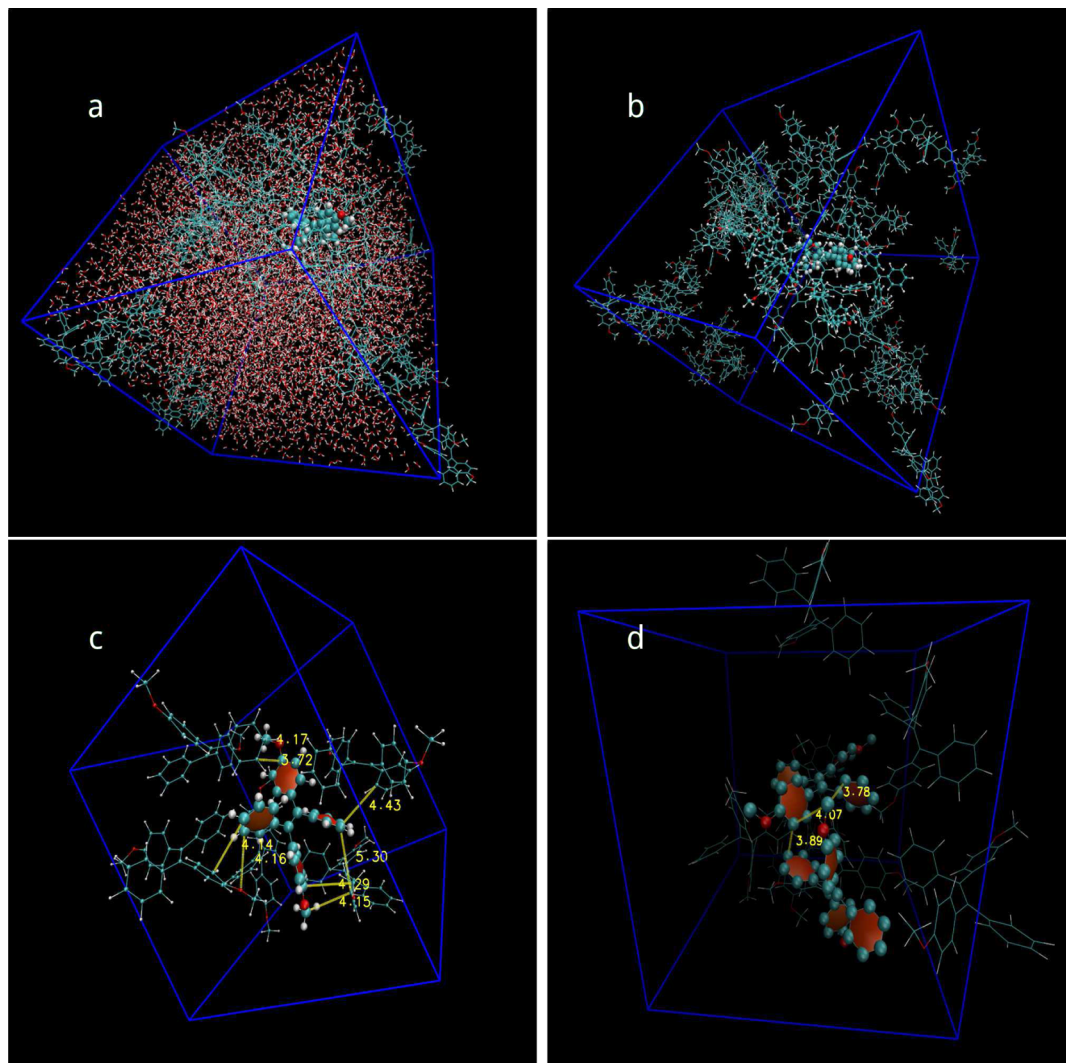


Figure 9. Geometry of the DMO-TPE molecule at the concentration of 1.97 mol % in water solution.

amplitudes of RDFs have a slight difference. The RDFs of DMO-TPE molecules themselves are very much dependent on the concentrations. At low concentration, there are three major peaks. Together with Figure 7, we find that the peaks at 0.7 and 0.8 nm represent the dimer aggregates with different arrangements, whereas other peaks are the average distance between block aggregates. At high concentration, the peak of dimer aggregates at 0.7 nm is dominant because the DMO-TPE molecules form a large aggregate with chain-type property.

3.3. Properties of DMO-TPE Aggregates. Once the stable conformations of aggregates in water solution are known, the QM/MM calculations can be performed to investigate the geometrical and electronic properties. As an example, Figures 9(a) and (b) separately show the DMO-TPE aggregates with and without water molecules at the snapshot of 10 ns at the concentration of 1.97 mol %. We first consider a single DMO-TPE molecule in aggregates as shown in Figure 9(c). The purpose of choosing this target molecule is to mimic its solid environment, because it is surrounded by the phenyl rings of neighboring DMO-TPE molecules with a close atom–atomic distance of about 4 Å. The conformation of this aggregates is already very different from that in the crystal structure where the average distance is about 8 Å (see Figure S2 in the SI). It is

thus expected that the AIE effect of amorphous conformation in solution may be different from that in the crystal structure.

To investigate the geometrical properties of this DMO-TPE molecule in the aggregated phase, we optimize its ground- and excited-state geometries by the QM/MM method. Here the other DMO-TPE and water molecules are treated by MM. The optimized geometrical parameters are shown in Table 1. In the ground state, the listed bond lengths are very close to those of the isolated molecule in vacuum, but the torsional angles show evident difference. The molecular symmetry is fully broken down in the aggregated phase, and the four torsional angles of benzyl rings show a large difference because of the amorphous conformation of aggregates in solution. The dihedral angles of benzyl groups are a little smaller than those of phenyl groups due to the H-bonds with the external methyl group. It seems that the steric hindrance of the other DMO-TPE molecules and water molecules limits the rotatable ability of the phenyl group. Unlike the free molecule, the DMO-TPE molecule in the aggregated environment does not alter much its molecular geometry upon the electronic excitation. The differences of the torsional angles in the optimized geometries between the ground and excited states for the molecule in the aggregated environment are much smaller than those in the free molecule,

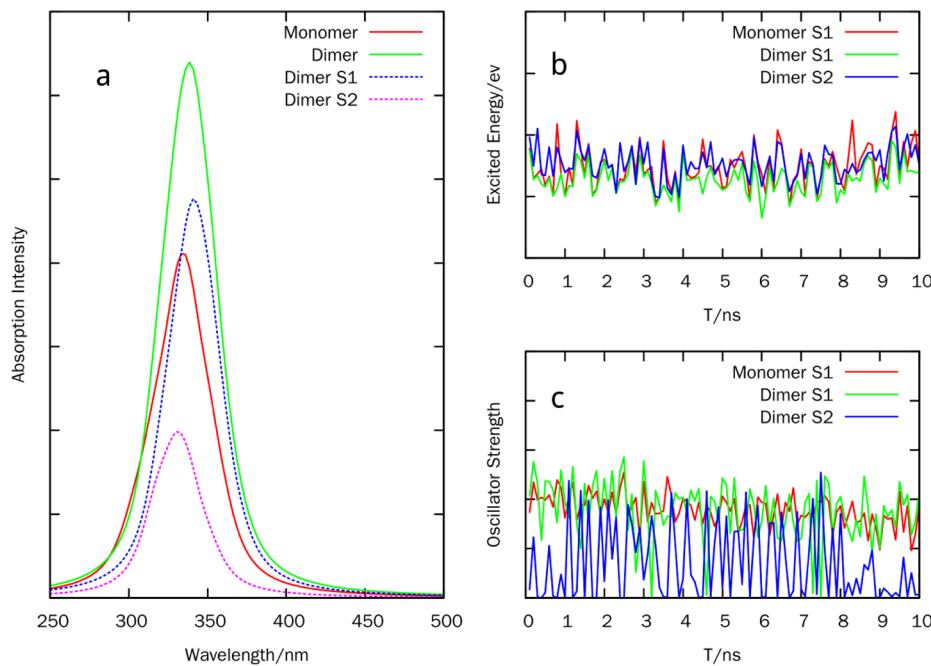


Figure 10. (a) Statistically averaged electronic absorption spectra of the DMO-TPE monomer and its dimer by the QM/MM method. (b) and (c) are the fluctuations of the two lowest excitation energies and oscillator strengths of dimer.

Table 3. Average Excitation Energies and Oscillator Strengths of the DMO-TPE Monomer and Dimer at Different Concentrations

parameter		values					
mol %		2.60	1.97	1.11	0.74	0.41	0.11
monomer	$\Delta E/\text{nm}$	340.086	331.631	325.577	328.959	337.398	334.626
	f	0.3580	0.3589	0.3435	0.3442	0.3757	0.3608
dimer	$\Delta E/\text{nm}$	340.932	334.824	335.889	335.206	338.532	338.102
	f	0.4907	0.4951	0.4028	0.4136	0.4734	0.4661

indicating that the condensed phase environment of the DMO-TPE constricts its intramolecular rotations.

At the optimized geometries, we have calculated the vertical absorption and emission energies as well as the corresponding oscillator strengths. The results are listed in Table 2, in which the corresponding quantities of the isolated DMO-TPE molecule in vacuum and water solution obtained by TDDFT and TDDFT/PCM are also shown for the comparison. The calculated absorption and emission energies in the aggregated phase are very close to the experimentally measured values.¹⁷ It is clear that the molecular environments have an evident effect on the light absorption and emission processes. However, their roles played on the absorption process are much smaller than those in the emission. In the absorption, the different molecular environments cause a small difference on the excitation energies and corresponding transition dipole moments, whereas, in the emission, the different molecular environments cause a huge difference on both the emission energies and corresponding transition dipoles. The maximum difference in the emission energies reaches to about 400 nm, and the oscillator strength changes from 0.16 (in vacuum) to 0.39 (in aggregation). Therefore, the molecular condensed phase environment evidently enhances the molecular emissive efficiency by increasing the transition dipole moments of the corresponding state.

Besides the RIR effect on AIE, we further calculate the spectra of a molecular dimer in the aggregated environment to

investigate the aggregation effect. The dimer consists of two adjacent DMO-TPE molecules as shown in Figure 9(d). To closely mimic the realistic condition in the experimental measurement, one has to consider the fluctuation of geometries caused by the concentration effect. We thus calculate the spectra with the use of the QM/MM method at the geometries (about 100 snapshots) obtained from the trajectories of MD simulation in 10 ns, and the obtained statistical average of spectra are shown in Figure 10(a), where the averaged spectra of the DMO-TPE monomer is also displayed for comparison. QM parts are calculated at the theoretical level of B3LYP/6-31G. It is seen that although the spectral line shapes of dimer and monomer are similar, the spectral position of the dimer has 5 nm redshift and the intensity is about 1.8-fold larger. The absorption intensity of the dimer's S₁ is 2-fold larger than that of the S₂, indicating that the dimer is more like the J-type aggregate,⁶⁸ which is consistent with a previous investigation.⁷ From the detailed fluctuations of energies and oscillator strengths, shown in Figure 10(b) and (c), it is found that the dimer indeed dominantly has a J-aggregation property although the fluctuations result in the partially mixed J- and H-aggregation. This dimer formed at about 0.8 ns, the distance between the center of mass of monomers is about 0.7 to 0.85 nm, and the oppositely aligned is almost 60° to 110°. The oscillation of the dimer structure agrees well with the mix of J- and H-aggregation. The more detailed RDF is listed in Figure S3 of the SI.

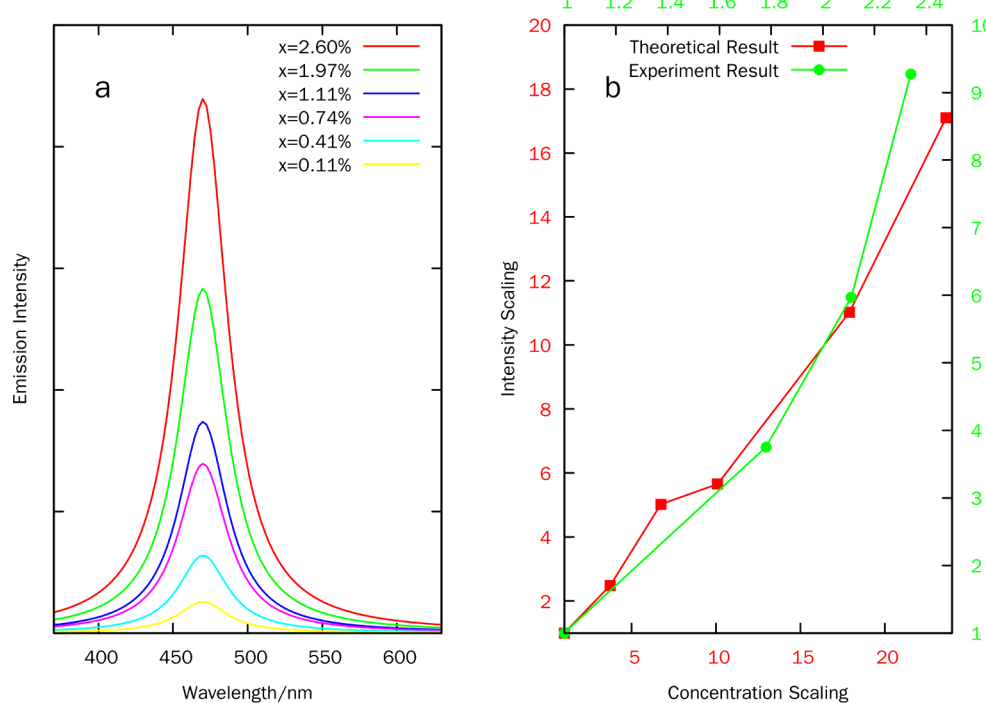


Figure 11. (a) Aggregate-induced emission spectra. (b) The concentration dependence of emission intensities.

It should be addressed that the absorption peaks of the DMO-TPE monomer and dimer in aggregates are evidently different from those in their isolated and crystal environment (see Figures S1 and S2 and Table S3 in the SI). For instance, the first absorption peak of the monomer is about 333 nm, whereas it becomes 360 nm in the isolated molecule shown in Figure 2. This large blueshift is caused by the RIR effect. The dimer also shows similar behaviors because the molecular distance in the dimer from the aggregates is smaller than that from pure water and crystals.

3.4. Concentration-Dependent Effect of the Spectra of DMO-TPE Aggregates. Table 3 lists the averaged excitation energies of first absorption peaks and oscillator strengths of the monomer and dimer at different concentrations. The spectral line shapes for the monomer and dimer in different concentrations are very similar to the fluctuations around 335 nm within 10 nm widths, consistent with the experimental value of 330 nm.¹⁷ However, the absorption intensities of dimers are about 1.5 times larger than those of the monomer, and its spectral positions have slight redshifts. These features manifest that the monomer and dimer geometries and electronic structures are very similar at different concentrations, the dimer has a J-aggregation behavior, and the aggregated induced absorption can be dominantly described by the monomer spectra in the aggregated phase.

To estimate the concentration dependence of emission, we can reasonably assume that the emission intensity is proportional to the number of DMO-TPE monomers in aggregate based on the above absorption properties. We first optimize the excited-state geometries of monomers chosen from the aggregate using the QM/MM method. After the statistical average, the obtained average emission energy is 470.07 nm, which is very close to the experimental value of 477 nm.¹⁷ Figure 11(a) displays the oscillator strengths with respect to the fluctuation of emission energy obtained from the MD trajectory at different concentrations. As expected, the higher concen-

tration leads to the stronger emission because of more monomers in the aggregates. Experimentally, the AIE is measured by increasing the water component in the water/AN mixture solution, where the effect of the high water fraction in the mixture solution is to assist in dissolving DMO-TPE molecules, leading to high concentration. We may thus make the quantitative comparison between experimental AIE and the present calculated results. We choose the calculated emission intensity at 0.11 mol % as a reference. The other spectral intensities and concentrations can be scaled accordingly. Similarly, the spectral intensity from the experimental measurement at 75% water fraction is taken as the reference because the obvious emission appears in this case. After scaling the concentrations and spectral intensities based on the references for the calculated and experimental results, it is found that both the AIE tendencies agree with each other quite well, as shown in Figure 11(b), indicating that the mechanism of AIE is correctly revealed.

4. CONCLUDING REMARKS

Combining MD simulations and QM/MM calculations, we have investigated the detailed aggregation processes and the AIE mechanism of DMO-TPE molecules in water solution, and several interesting results are obtained.

The time scale of aggregation process is at several nanoseconds. The sizes of molecular aggregates are very much dependent on the concentration. At low concentration, the aggregates show isolated block structures, whereas the large aggregates are formed with the chain-type structures at high concentration. Furthermore, the water molecules are evidently involved in the aggregates because two types of explicit hydrogen bonds are built between the waters and the phenyl groups as well as the methoxy groups of the DMO-TPE molecule. These simulated time scales and aggregation conformations may be helpful in synthesizing aggregates with tunable properties.

The molecular environment plays a significant role on the molecular geometries. For the isolated molecule in vacuo and solution, electronic excitation induces evident intramolecular rotation. The maximum difference in the dihedral angles between S_0 and S_1 geometries reaches 55° . In the aggregated phase, the molecular symmetry is fully broken down, and the intermolecular distance between the two neighboring DMO-TPE molecules is slightly shorter than that in the crystal. The effect of electronic excitation on the molecular geometries of the aggregates is much smaller than that on the isolated molecule. The RIR effect is evident in the aggregated phase, and it limits the rotational angles of phenyl rings within $2\text{--}10^\circ$ rather than $20\text{--}55^\circ$ in vacuo.

The calculations on the spectra have revealed that the monomer and dimer in aggregates essentially have similar absorption and emissive spectral line shapes but different concentration-dependent spectral intensities. The dimer's spectra have a slight redshift compared with the monomer and show the properties of J-type aggregation. The calculated absorption and emission energies in the aggregated phase are very close to the experimental results. The gradually increasing oscillator strength in the corresponding emission process by the solution concentration indicates that the AIE dominantly comes from the RIR effect as well as J-type aggregation behaviors. The molecular condensed phase environment largely restricts the intramolecular rotation, increases the transition dipoles of the corresponding emission process, and subsequently enhances the emission efficiency. Based on this mechanism, we have further calculated the concentration dependence of emission intensity, which is also quantitatively consistent with experimental measurement. Further investigations of AIE in mixture solutions, such as water/AN used in the experimental measurement, will be done in future work.

ASSOCIATED CONTENT

Supporting Information

The force field parameters of the DMO-TPE molecule, geometrical parameters and electronic absorption spectra of monomer and dimer of DMO-TPE molecules in aggregates and crystal are given out. The hydrogen-bond models and different molecular orientations of the dimers and the detailed RDFs in aggregates are shown. This material is available free of charge via the Internet at <http://pubs.acs.org>.

AUTHOR INFORMATION

Corresponding Authors

*E-mail: yizhao@xmu.edu.cn.

*E-mail: liangwz@xmu.edu.cn.

Notes

The authors declare no competing financial interest.

ACKNOWLEDGMENTS

The work is partially supported by National Science Foundation of China (Grant No. 21373163 and No. 21290193), National Basic Research Program of China (Grant No. 2011CB808501), and Research Foundation for the Doctoral Program of Higher Education of China. The partial numerical calculations have been done on the supercomputer systems in the supercomputer centers of USTC.

REFERENCES

- (1) Birks, J. B. *Photophysics of Aromatic Molecules*; Studies in the History of American Education Series; Wiley: 1970.
- (2) Jenekhe, S. A.; Osaheni, J. A. Excimers and exciplexes of conjugated polymers. *Science* **1994**, *265*, 765–768.
- (3) Friend, R. H.; Gymer, R. W.; Holmes, A. B.; Burroughes, J. H.; Marks, R. N.; Taliani, C.; Bradley, D.; Dos Santos, D. A.; Bredas, J. L.; Lögdlund, M. Electroluminescence in conjugated polymers. *Nature* **1999**, *397*, 121–128.
- (4) Chen, C. T. Evolution of red organic light-emitting diodes: materials and devices. *Chem. Mater.* **2004**, *16*, 4389–4400.
- (5) Luo, J. D.; Xie, Z. L.; Lam, J. W. Y.; Cheng, L.; Tang, B. Z.; Chen, H. Y.; Qiu, C. F.; Kwok, H. S.; Zhan, X. W.; Liu, Y. Q.; Zhu, D. B. Aggregation-induced emission of 1-methyl-1,2,3,4,5-pentaphenylsilole. *Chem. Commun.* **2001**, *381*, 1740–1741.
- (6) Hong, Y. N.; Lam, J. W. Y.; Tang, B. Z. Aggregation-induced emission. *Chem. Soc. Rev.* **2011**, *40*, 5361–5388.
- (7) Zhang, S.; Qin, A. J.; Sun, J. Z.; Tang, B. Z. Mechanism study of aggregation-induced emission. *Prog. Chem.* **2011**, *23*, 623–636.
- (8) Hong, Y. N.; Lam, J. W. Y.; Tang, B. Z. Aggregation-induced emission: phenomenon, mechanism and applications. *Chem. Commun.* **2009**, *4332*–4353.
- (9) Liu, J. Z.; Lam, J. W. Y.; Tang, B. Z. Aggregation-induced Emission of Silole Molecules and Polymers: Fundamental and Applications. *J. Inorg. Organomet. Polym.* **2009**, *19*, 249–285.
- (10) Wang, M.; Zhang, G. X.; Zhang, D. Q.; Zhu, D. B.; Tang, B. Z. Fluorescent bio/chemosensors based on silole and tetraphenylethene luminogens with aggregation-induced emission feature. *J. Mater. Chem.* **2010**, *20*, 1858–1867.
- (11) Qian, L. J.; Zhi, J. G.; Tong, B.; Yang, F.; Zhao, W.; Dong, Y. P. Organic compounds with aggregation-induced emission. *Prog. Chem.* **2008**, *20*, 673–678.
- (12) Qian, Y.; Xie, L. H.; Wang, S. Q.; Yang, G. Q. Progress in Organic Compounds with Aggregation Induced Enhanced Emission. *J. Nanjing Univ. Posts Telecommun. (Nat. Sci.)* **2008**, *28*, 1–8.
- (13) Yan, J.; Qin, A.; Sun, J. Z.; Tang, B. Z. Application of AIE-active molecules in biosensing. *China Sci. Bull.* **2010**, *55*, 1206–1213.
- (14) Zhao, Y. S.; Fu, H. B.; Peng, A. D.; Ma, Y.; Xiao, D. B.; Yao, J. N. Low-Dimensional Nanomaterials Based on Small Organic Molecules: Preparation and Optoelectronic Properties. *Adv. Mater.* **2008**, *20*, 2859–2876.
- (15) Leclerc, N.; Gravel, C.; Hawkes, R. Organic fluorophores exhibiting highly efficient photoluminescence in the solid state. *Chem.-Asian J.* **2010**, *5*, 1516–1531.
- (16) Qin, A. J.; Lam, J. W. Y.; Tang, B. Z. Click polymerization. *Chem. Soc. Rev.* **2010**, *39*, 2522–2544.
- (17) Tong, H.; Hong, Y. N.; Dong, Y. Q.; Häussler, M.; Li, Z.; Lam, J. W. Y.; Dong, Y. P.; Sung, H. H.-Y.; Williams, I. D.; Tang, B. Z. Protein detection and quantitation by tetraphenylethene-based fluorescent probes with aggregation-induced emission characteristics. *J. Phys. Chem. B* **2007**, *111*, 11817–11823.
- (18) Zijlstra, R. W.; van Duijnen, P. T.; Feringa, B. L.; Steffen, T.; Duppen, K.; Wiersma, D. A. Excited-state dynamics of tetraphenylethylene: Ultrafast Stokes shift, isomerization, and charge separation. *J. Phys. Chem. A* **1997**, *101*, 9828–9836.
- (19) Dong, Y. Q.; Lam, J. W. Y.; Qin, A. J.; Liu, J. Z.; Li, Z.; Tang, B. Z.; Sun, J. X.; Kwok, H. S. Aggregation-induced emissions of tetraphenylethene derivatives and their utilities as chemical vapor sensors and in organic light-emitting diodes. *Appl. Phys. Lett.* **2007**, *91*, 011111.
- (20) Nakamura, M.; Sanji, T.; Tanaka, M. Fluorometric Sensing of Biogenic Amines with Aggregation-Induced Emission-Active Tetraphenylethenes. *Chem. - Eur. J.* **2011**, *17*, 5344–5349.
- (21) Bian, N.; Chen, Q.; Qiu, X. L.; Qi, A. D.; Han, B. H. Imidazole-bearing tetraphenylethylene: fluorescent probe for metal ions based on AIE feature. *New J. Chem.* **2011**, *35*, 1667–1671.
- (22) Zhao, Z. J.; Lu, P.; Lam, J. W. Y.; Wang, Z. M.; Chan, C. Y. K.; Sung, H. H. Y.; Williams, I. D.; Ma, Y. G.; Tang, B. Z. Molecular anchors in the solid state: Restriction of intramolecular rotation boosts

- emission efficiency of luminogen aggregates to unity. *Chem. Sci.* **2011**, *2*, 672–675.
- (23) Shustova, N. B.; Ong, T.-C.; Cozzolino, A. F.; Michaelis, V. K.; Griffin, R. G.; Dinca, M. Phenyl Ring Dynamics in a Tetraphenylethylene-Bridged Metal-Organic Framework: Implications for the Mechanism of Aggregation-Induced Emission. *J. Am. Chem. Soc.* **2012**, *134*, 15061–15070.
- (24) Zhao, G. J.; Han, K. L.; Lei, Y. B.; Dou, Y. S. Ultrafast excited-state dynamics of tetraphenylethylene studied by semiclassical simulation. *J. Chem. Phys.* **2007**, *127*, 094307.
- (25) Wu, Q. Y.; Peng, Q.; Niu, Y. L.; Gao, X.; Shuai, Z. G. Theoretical insights into the aggregation-induced emission by hydrogen bonding: a QM/MM study. *J. Phys. Chem. A* **2012**, *116*, 3881–3888.
- (26) Wang, J.; Mei, J.; Hu, R. R.; Sun, J. Z.; Qin, A. J.; Tang, B. Z. Click synthesis, aggregation-induced emission, E/Z isomerization, self-organization, and multiple chromisms of pure stereoisomers of a tetraphenylethene-cored luminogen. *J. Am. Chem. Soc.* **2012**, *134*, 9956–9966.
- (27) He, B. R.; Ye, S. H.; Guo, Y. J.; Chen, B.; Xu, X. F.; Qiu, H. Y.; Zhao, Z. J. Aggregation-enhanced emission and efficient electroluminescence of conjugated polymers containing tetraphenylethene units. *Sci. China Chem.* **2013**, *56*, 1221–1227.
- (28) Huang, J.; Chen, P. Y.; Yang, X.; Tang, R. L.; Wang, L.; Qin, J. Q.; Li, Z. Construction of deep-blue AIE luminogens with TPE and oxadiazole units. *Sci. China Chem.* **2013**, *56*, 1213–1220.
- (29) Chen, J. W.; Law, C. C. W.; Lam, J. W. Y.; Dong, Y. P.; Lo, S. M. F.; Williams, I. D.; Zhu, D. B.; Tang, B. Z. Synthesis, light emission, nanoaggregation, and restricted intramolecular rotation of 1,1-substituted 2,3,4,5-tetraphenylsiloles. *Chem. Mater.* **2003**, *15*, 1535–1546.
- (30) Ryu, S. Y.; Kim, S.; Seo, J.; Kim, Y.-W.; Kwon, O.-H.; Jang, D.-J.; Park, S. Y. Strong fluorescence emission induced by supramolecular assembly and gelation: luminescent organogel from non emissive oxadiazole-based benzene-1,3,5-tricarboxamide gelator. *Chem. Commun.* **2004**, *1*, 70–71.
- (31) Lenoble, G.; Lacaze-Dufaure, C.; Urrutigoity, M.; Mijoule, C.; Kalck, P. Tandem Palladium-Catalyzed Cyclocarbonylation of Isolimonene: A Mechanistic Investigation and Theoretical Calculations on the Fully Diastereoselective Step. *Eur. J. Inorg. Chem.* **2004**, *2004*, 791–797.
- (32) Tong, H.; Dong, Y. Q.; Häußler, M.; Lam, J. W. Y.; Sung, H. H.-Y.; Williams, I. D.; Sun, J. Z.; Tang, B. Z. Tunable aggregation-induced emission of diphenyldibenzofulvenes. *Chem. Commun.* **2006**, *10*, 1133–1135.
- (33) Hu, R. R.; Lager, E.; Aguilar-Aguilar, A.; Liu, J. Z.; Lam, J. W. Y.; Sung, H. H. Y.; Williams, I. D.; Zhong, Y. C.; Wong, K. S.; Pena-Cabrera, E. Twisted intramolecular charge transfer and aggregation-induced emission of BODIPY derivatives. *J. Phys. Chem. C* **2009**, *113*, 15845–15853.
- (34) Itami, K.; Ohashi, Y.; Yoshida, J.-I. Triarylethene-based extended π -systems: programmable synthesis and photophysical properties. *J. Org. Chem.* **2005**, *70*, 2778–2792.
- (35) Wang, Z. X.; Shao, H. X.; Ye, J. C.; Tang, L.; Lu, P. Dibenzosuberenyldiene-ended fluorophores: Rapid and efficient synthesis, characterization, and aggregation-induced emissions. *J. Phys. Chem. B* **2005**, *109*, 19627–19633.
- (36) Kim, S.; Zheng, Q. D.; He, G. S.; Bharali, D. J.; Pudavar, H. E.; Baev, A.; Prasad, P. N. Aggregation-Enhanced Fluorescence and Two-Photon Absorption in Nanoaggregates of a 9,10-Bis[4'-(4'-aminostyryl)styryl]anthracene Derivative. *Adv. Funct. Mater.* **2006**, *16*, 2317–2323.
- (37) He, J. T.; Xu, B.; Chen, F. P.; Xia, H. J.; Li, K. P.; Ye, L.; Tian, W. J. Aggregation-induced emission in the crystals of 9,10-distyrylanthracene derivatives: the essential role of restricted intramolecular torsion. *J. Phys. Chem. C* **2009**, *113*, 9892–9899.
- (38) Shimizu, M.; Tatsumi, H.; Mochida, K.; Shimono, K.; Hiyama, T. Synthesis, Crystal Structure, and Photophysical Properties of (1E,3E,SE)-1,3,4,6-Tetraarylhexa-1,3,5-trienes: A New Class of Fluorophores Exhibiting Aggregation-Induced Emission. *Chem. - Asian J.* **2009**, *4*, 1289–1297.
- (39) Tang, B. Z. Photoluminescence and electroluminescence of hexaphenylsilole are enhanced by pressurization in the solid state. *Chem. Commun.* **2008**, *26*, 2989–2991.
- (40) Ren, Y.; Lam, J. W. Y.; Dong, Y. Q.; Tang, B. Z.; Wong, K. S. Enhanced emission efficiency and excited state lifetime due to restricted intramolecular motion in silole aggregates. *J. Phys. Chem. B* **2005**, *109*, 1135–1140.
- (41) Ren, Y.; Dong, Y. Q.; Lam, J. W. Y.; Tang, B. Z.; Wong, K. S. Studies on the aggregation-induced emission of silole film and crystal by time-resolved fluorescence technique. *Chem. Phys. Lett.* **2005**, *402*, 468–473.
- (42) Wang, Z. S.; Hara, K.; Danoh, Y.; Kasada, C.; Shinpo, A.; Suga, S.; Arakawa, H.; Sugihara, H. Photophysical and (photo) electrochemical properties of a coumarin dye. *J. Phys. Chem. B* **2005**, *109*, 3907–3914.
- (43) Sherrill, C. D.; Takatani, T.; Hohenstein, E. G. An Assessment of Theoretical Methods for Nonbonded Interactions: Comparison to Complete Basis Set Limit Coupled-Cluster Potential Energy Curves for the Benzene Dimer, the Methane Dimer, Benzene-Methane, and Benzene-H₂S. *J. Phys. Chem. A* **2009**, *113*, 10146–10159.
- (44) Lenderink, E.; Duppen, K.; Wiersma, D. A. Femtosecond Twisting and Coherent vibrational motion in the excited state of tetraphenylethylene. *J. Phys. Chem.* **1995**, *99*, 8972–8977.
- (45) Zhao, G. J.; Han, K. L.; Lei, Y. B.; Dou, Y. S. Ultrafast excited-state dynamics of tetraphenylethylene studied by semiclassical simulation. *J. Chem. Phys.* **2007**, *127*, 094307.
- (46) Gagnon, E.; Maris, T.; Arseneault, P.-M.; Maly, K. E.; Wuest, J. D. Structural features in crystals of derivatives of benzene with multiple contiguous phenyl substituents. *Cryst. Growth Des.* **2009**, *10*, 648–657.
- (47) Barbara, P. F.; Rand, S. D.; Rentzepis, P. M. Direct measurements of tetraphenylethylene torsional motion by picosecond spectroscopy. *J. Am. Chem. Soc.* **1981**, *103*, 2156–2162.
- (48) Gao, X.; Peng, Q.; Niu, Y. L.; Wang, D.; Shuai, Z. G. Theoretical insight into the aggregation induced emission phenomena of diphenyldibenzofulvene: a nonadiabatic molecular dynamics study. *Phys. Chem. Chem. Phys.* **2012**, *14*, 14207–14216.
- (49) Jiang, Y. Q.; Peng, Q.; Gao, X.; Shuai, Z. G.; Niu, Y. L.; Lin, S. H. Theoretical design of polythiénylenevinylene derivatives for improvements of light-emitting and photovoltaic performances. *J. Mater. Chem.* **2012**, *22*, 4491–4501.
- (50) Wu, Q. Y.; Zhang, T.; Peng, Q.; Wang, D.; Shuai, Z. G. Aggregation induced blue-shifted emission—the molecular picture from a QM/MM study. *Phys. Chem. Chem. Phys.* **2014**, *16*, 5545–5552.
- (51) McMurry, J. E. Carbonyl-coupling reactions using low-valent titanium. *Chem. Rev.* **1989**, *89*, 1513–1524.
- (52) Pronk, S.; Pál, S.; Schulz, R.; Larsson, P.; Bjelkmar, P.; Apostolov, R.; Shirts, M. R.; Smith, J. C.; Kasson, P. M.; van der Spoel, D. GROMACS 4.5: a high-throughput and highly parallel open source molecular simulation toolkit. *Bioinformatics* **2013**, *29*, 845–854.
- (53) Frisch, M. J.; Trucks, G. W.; Schlegel, H. B.; Scuseria, G. E.; Robb, M. A.; Cheeseman, J. R.; Scalmani, G.; Barone, V.; Mennucci, B.; Petersson, G. A.; Nakatsuji, H.; Caricato, M.; Li, X.; Hratchian, H. P.; Izmaylov, A. F.; Bloino, J.; Zheng, G.; Sonnenberg, J. L.; Hada, M.; Ehara, M.; Toyota, K.; Fukuda, R.; Hasegawa, J.; Ishida, M.; Nakajima, T.; Honda, Y.; Kitao, O.; Nakai, H.; Vreven, T.; Montgomery, J. A., Jr.; Peralta, J. E.; Ogliaro, F.; Bearpark, M.; Heyd, J. J.; Brothers, E.; Kudin, K. N.; Staroverov, V. N.; Kobayashi, R.; Normand, J.; Raghavachari, K.; Rendell, A.; Burant, J. C.; Iyengar, S. S.; Tomasi, J.; Cossi, M.; Rega, N.; Millam, J. M.; Klene, M.; Knox, J. E.; Cross, J. B.; Bakken, V.; Adamo, C.; Jaramillo, J.; Gomperts, R.; Stratmann, R. E.; Yazayev, O.; Austin, A. J.; Cammi, R.; Pomelli, C.; Ochterski, J. W.; Martin, R. L.; Morokuma, K.; Zakrzewski, V. G.; Voth, G. A.; Salvador, P.; Dannenberg, J. J.; Dapprich, S.; Daniels, A. D.; Farkas, O.; Foresman, J. B.; Ortiz, J. V.; Cioslowski, J.; Fox, D. J. *Gaussian 09*, revision B. 01; Gaussian, Inc.: Wallingford, CT, 2009.

- (54) Rappé, A. K.; Casewit, C. J.; Colwell, K.; Goddard, W., III; Skiff, W. UFF, a full periodic table force field for molecular mechanics and molecular dynamics simulations. *J. Am. Chem. Soc.* **1992**, *114*, 10024–10035.
- (55) Jorgensen, W. L.; Chandrasekhar, J.; Madura, J. D.; Impey, R. W.; Klein, M. L. Comparison of simple potential functions for simulating liquid water. *J. Chem. Phys.* **1983**, *79*, 926–935.
- (56) Darden, T.; York, D.; Pedersen, L. Particle mesh Ewald: An $N \log(N)$ method for Ewald sums in large systems. *J. Chem. Phys.* **1993**, *98*, 10089–10092.
- (57) Essmann, U.; Perera, L.; Berkowitz, M. L.; Darden, T.; Lee, H.; Pedersen, L. G. A smooth particle mesh Ewald method. *J. Chem. Phys.* **1995**, *103*, 8577–8593.
- (58) Berendsen, H. J.; Postma, J. P. M.; van Gunsteren, W. F.; DiNola, A.; Haak, J. Molecular dynamics with coupling to an external bath. *J. Chem. Phys.* **1984**, *81*, 3684–3690.
- (59) Dapprich, S.; Komáromi, I.; Byun, K. S.; Morokuma, K.; Frisch, M. J. A new ONIOM implementation in Gaussian98. Part I. The calculation of energies, gradients, vibrational frequencies and electric field derivatives. *J. Mol. Struct.: THEOCHEM* **1999**, *461*, 1–21.
- (60) Vreven, T.; Frisch, M.; Kudin, K.; Schlegel, H.; Morokuma, K. Geometry optimization with QM/MM methods II: Explicit quadratic coupling. *Mol. Phys.* **2006**, *104*, 701–714.
- (61) Tomasi, J.; Mennucci, B.; Cammi, R. Quantum mechanical continuum solvation models. *Chem. Rev.* **2005**, *105*, 2999–3094.
- (62) Cammi, R.; Mennucci, B. Linear response theory for the polarizable continuum model. *J. Chem. Phys.* **1999**, *110*, 9877–9886.
- (63) Cossi, M.; Barone, V. Time-dependent density functional theory for molecules in liquid solutions. *J. Chem. Phys.* **2001**, *115*, 4708–4717.
- (64) Improta, R.; Barone, V.; Scalmani, G.; Frisch, M. J. A state-specific polarizable continuum model time dependent density functional theory method for excited state calculations in solution. *J. Chem. Phys.* **2006**, *125*, 054103.
- (65) Improta, R.; Scalmani, G.; Frisch, M. J.; Barone, V. Toward effective and reliable fluorescence energies in solution by a new state specific polarizable continuum model time dependent density functional theory approach. *J. Chem. Phys.* **2007**, *127*, 074504.
- (66) Head-Gordon, M.; Rico, R. J.; Oumi, M.; Lee, T. J. A doubles correction to electronic excited states from configuration interaction in the space of single substitutions. *Chem. Phys. Lett.* **1994**, *219*, 21–29.
- (67) Head-Gordon, M.; Maurice, D.; Oumi, M. A perturbative correction to restricted open shell configuration interaction with single substitutions for excited states of radicals. *Chem. Phys. Lett.* **1995**, *246*, 114–121.
- (68) Kasha, M.; Rawls, H. R.; Ashraf El-Bayoumi, M. The exciton model in molecular spectroscopy. *Pure Appl. Chem.* **1965**, *11*, 371–392.